Energetics of Intermolecular Hydrogen Bonds in a Hydrophobic Protein Cavity

Lan Liu,[1] Alyson Baergen,[1] Klaus Michelsen,[2] Elena N. Kitova,[1] Paul D. Schnier[3] and John S. Klassen[1]

[1]*Alberta Glycomics Centre and Department of Chemistry, University of Alberta, Edmonton, Alberta, Canada T6G 2G2*

[2]*Molecular Structure, Amgen, Cambridge, MA 02142*

[3]*Molecular Structure, Amgen, South San Francisco, CA 94080*

Abstract

This work explores the energetics of intermolecular H-bonds inside a hydrophobic protein cavity. Kinetic measurements were performed on the gaseous deprotonated ions (at the -7 charge state) of complexes of bovine β-lactoglobulin (Lg) and three monohydroxylated analogs of palmitic acid (PA): 3-hydroxypalmitic acid (3-OHPA), 7-hydroxypalmitic acid (7-OHPA) and 16-hydroxypalmitic acid (16-OHPA). From the increase in the activation energy for the dissociation of the $(Lg + X\text{-}OHPA)^{7-}$ ions, compared with that of the $(Lg + PA)^{7-}$ ion, it is concluded that the –OH groups of the X-OHPA ligands participate in strong (5 – 11 kcal mol^{-1}) intermolecular H-bonds in the hydrophobic cavity of Lg. The results of molecular dynamics (MD) simulations suggest that the –OH groups of 3-OHPA and 16-OHPA act as H-bond donors and interact with backbone carbonyl oxygens, while the –OH group of 7-OHPA acts as both H-bond donor and acceptor with nearby side chains. Interestingly, the capacity for intermolecular H-bonds within the Lg cavity, as suggested by the gas-phase measurements, does not necessarily lead to enhanced binding in aqueous solution. The association constant (K_a) measured for 7-OHPA ($(2.3\pm0.2)\times10^5$ M^{-1}) is similar to the value for the PA ($(3.8\pm0.1)\times10^5$ M^{-1}); K_a for 3-OHPA ($(1.1\pm0.3)\times10^6$ M^{-1}) is approximately three-times larger, while K_a for 16-OHPA ($(2.3\pm0.2)\times10^4$ M^{-1}) is an order of magnitude smaller. Taken together, the results of this study suggest that the energetics of the intermolecular H-bonds are similar in magnitude to the energetic penalties for desolvating the ligand –OH groups.

Introduction

Hydrophobic bonding, which refers to the attraction of non-polar molecules or moieties in water, plays an important role in biomolecular recognition (e.g. the binding of small molecules to their protein receptors) and protein hydrophobic surfaces and cavities represent attractive targets for drug development [1-4]. The concomitant formation of intermolecular hydrogen bonds (H-bonds) can also modulate both the kinetic and thermodynamic stability of hydrophobic protein-ligand interactions [5,6]. Indeed, it has been suggested that so-called "super affinities" arise when ligand interactions within hydrophobic protein enclosures are accompanied by the formation of H-bonds [7]. Consequently, the capacity of amino acid residues, within hydrophobic regions, to engage in intermolecular H-bonds and the strength of the resulting interactions are of significant fundamental and applied interest. However, delineating the energetic contributions of specific protein-ligand intermolecular interactions from the influence of solvent reorganization remains a significant experimental challenge and, at present, quantitative data are lacking.

Gas-phase studies of the kinetic stability of structurally related protein-ligand complexes represent a promising experimental strategy to quantify the strength of intermolecular interactions, free of solvent effects [8-14]. Furthermore, insights into solvent effects may be gained from a comparison of the kinetic stabilities of protein-ligand complexes in their hydrated (solution) and dehydrated (gas-phase) states [11,12,14]. For example, using the blackbody infrared radiative dissociation–functional group replacement (BIRD-FGR) method [8-14], the intermolecular interactions in the gaseous ions of protein-ligand complexes composed of a single chain antibody (scFv), a

model carbohydrate binding protein, and a trisaccharide ligand (α-D-Gal*p*-(1→2)-[α-D-Abe*p*-(1→3)]-α-D-Man*p*-OCH_3) [8,9], β-lactoglobulin (Lg), a model lipid-binding protein, and fatty acids (FAs) [10-12], and streptavidin homotetramer (S_4) and its high affinity ligand biotin (B), were recently elucidated and quantified [13,14]. Results obtained for protonated (scFv + α-D-Gal*p*-(1→2)-[α-D-Abe*p*-(1→3)]-α-D-Man*p*-OCH_3)$^{n+}$ ions revealed that some of the specific intermolecular H-bonds are conserved upon transfer of the complex from solution to the gas phase by electrospray ionization (ESI) [8,9]. Kinetic data measured for the loss of FA from deprotonated (Lg + FA)$^{n-}$ ions suggest that the ligand acyl chain is retained within the hydrophobic cavity of Lg in the gas phase [10]. A comparison of dissociation rate constants measured at 25°C in the gas phase and in aqueous solution revealed that (Lg + FA) complexes are more stable kinetically in the absence of water [11]. Furthermore, a comparison of the gas-phase dissociation activation energies (E_a) with enthalpies reported for the transfer of hydrocarbons from the gas phase to various organic solvents led to the intriguing conclusion that the cavity of Lg is relatively polar in nature [12]. Measurements of the kinetics for B loss from protonated (S_4 + 4B)$^{n+}$ ions, together with the results of molecular dynamics (MD) simulations, suggest that solution specific intermolecular H-bonds and van der Waals contacts are preserved in the gas phase [13]. It was also shown that the differences in E_a values measured for the gaseous complex ions and solvated complex can be accounted for by the rehydration of B in the dissociative transition state (*TS*) [14].

The results of the aforementioned studies highlight the power of gas-phase kinetic measurements to reveal new insights, inaccessible by other methods, into the forces

responsible for the stabilities of protein-ligand complexes. Here, we apply this general strategy to probe, for the first time, the energetics of intermolecular H-bonds within a hydrophobic protein cavity. Lg, which possesses a large, dry (in absence of ligand) hydrophobic cavity, lined with 12 aliphatic residues (Leu^{58}, Val^{41}, Val^{43}, Leu^{46}, Leu^{54}, Ile^{56}, Leu^{58}, Ile^{71}, Leu^{87}, Val^{92} and Leu^{103}) and one aromatic residue (Phe^{105}) [15-17], and its interactions with three monohydroxylated analogs of palmitic acid (PA): 3-hydroxypalmitic acid (3-OHPA), 7-hydroxypalmitic acid (7-OHPA) and 16-hydroxypalmitic acid (16-OHPA), served as model systems for this study (Figure 1). The direct ESI mass spectrometry (MS) binding assay [18] and surface plasmon resonance (SPR) spectroscopy were employed to assess the influence of the ligand -OH groups on the thermodynamic and kinetic stabilities of the (Lg + X-OHPA) complexes in aqueous solution. Arrhenius parameters for ligand loss from the gaseous $(Lg + X\text{-}OHPA)^{7-}$ ions were measured using BIRD [19,20]. Extensive efforts to produce crystal structures for the (Lg + X-OHPA) complexes were unsuccessful. Consequently, molecular dynamics (MD) simulations were performed on each of the hydrated (Lg + X-OHPA) complexes, as well as the gaseous $(Lg + X\text{-}OHPA)^{7-}$ ions, to suggest possible intermolecular H-bonds involving the ligand -OH groups.

Experimental

Protein and ligand

Bovine β-lactoglobulin (Lg, monomer MW 18281 Da), 3-hydroxypalmitic acid (3-OHPA), 16-hydroxypalmitic acid (16-OHPA), were purchased from Sigma-Aldrich Canada (Oakville, Canada). 7-hydroxypalmitic acid (7-OHPA) was purchased from Larodan Fine Chemical (Malmö, Sweden). The Lg was dissolved and exchanged directly

into Milli-Q water, using an Amicon microconcentrator with a 10 kDa molecular weight cut-off, followed by filtration using an Amicon ultra centrifugal filter with a molecular weight cutoff of 100 kDa to remove Lg aggregates. Lyophilizing a known volume of the filtrate and measuring the mass of the protein was used to determine the concentration of Lg. The protein stock solution was stored at -20 °C until needed. Ligand stock solutions were prepared by dissolving each X-OHPA into aqueous ammonium acetate (25 mM). For ESI, solutions were prepared from aqueous stock solutions of protein and ligand. Aqueous ammonium hydroxide was added to adjust the pH to 8.5; imidazole (10 mM) was also added in order to minimize the occurrence of in-source dissociation [18].

Mass spectrometry

Mass spectra were acquired on a 9.4T Apex II FTICR mass spectrometer (Bruker, Billerica, MA) equipped with a nanoflow ESI ion source. Complete details of the instrumental and experimental conditions used for the BIRD measurements and the direct ESI-MS affinity measurements can be found elsewhere, along with descriptions of how the kinetic and affinity data were analyzed [10,18].

Surface plasmon resonance

The SPR experiments were conducted on a Biacore T200 instrument (GE Healthcare) at 25°C. Interactions between Lg and X-OHPA were measured in a buffer (pH 8.0) compromised of 25 mM tris(hydroxymethyl)aminomethane (Tris), 1 mM TCEP, 0.2 mM 3-[(3-cholamidopropyl)dimethylammonio]-1-propanesulfonate (CHAPS), and 8% (v/v) ethanol. Complete details of the experimental conditions can be found elsewhere [12].

Molecular dynamic (MD) simulations

MD simulations were performed using the InsightII program suite (Accelrys, San Diego, CA). The crystal structure of the (Lg + PA) complex (PDB 1B0O) was used to construct the initial geometry of the (Lg + X-OHPA) complexes, where X = 3, 7 and 16. The simulations were performed using the Consistent Valence Force Field (CVFF). For simulations in the gas phase, a charge configuration (deprotonated residues: Asp^{53}, Asp^{85}, Asp^{98}, Asp^{130}, Glu^{45}, Glu^{114}, Glu^{158}) that leads to the "open" structure, in which the ligand carboxyl group does not participate in any strong H-bonds, was used [10]. Several ligand positions were used to generate different starting structures of complex ions for the MD simulations. The energies of the $(Lg + X\text{-}OHPA)^{7-}$ ions were minimized by the steepest gradient methods (1000 iterations), followed by conjugate gradient method (10000 iterations) using a 0.001 kcal $mol^{-1}Å^{-1}$ convergence criterion. At the start of the simulation, the system was equilibrated at 300 K for 1 ps, with a time step of 1 fs. After this, production dynamics were performed for 2.5 ns and data collected every 250 fs. For the solvated complexes, each (Lg + X-OHPA) complex was centered in a cubic (70 Å x 70 Å x 70 Å) water box. All of the acidic amino acid residues on the Lg surface were deprotonated and all basic residues were protonated. The overall charge on Lg was -8; the X-OHPA ligands were also deprotonated. Nine Na^+ counter ions were added into water box to neutralize the system. After 10000 steps minimization, the simulation was first run at constant volume (NVT) with periodic boundary conditions (PBC) at 300 K for 5000 fs, followed by simulation at constant pressure (NPT, 1 bar) with PBC at 300 K for 1.0 ns. The dynamics data were collected every 1000 fs.

Results and discussion

Stability of the (Lg + X-OHPA) complexes in aqueous solution

Gaseous deprotonated ions of the (Lg + X-OHPA) complexes were detected by ESI-MS performed in negative ion mode on aqueous ammonium acetate (10 mM) solutions of Lg (12 - 15 μM) and X-OHPA (9 μM for 3-OHPA and 7-OHPA, and 24 μM for 16-OHPA) at 25 °C and pH 8.5 (Figure 2). Imidazole (10 mM), which is known to minimize the extent of in-source (gas-phase) dissociation of protein complexes during ESI, was also added to each solution [18,21,22]. From the relative abundances of the ligand-bound and free (unbound) Lg ions, the affinities of each of the X-OHPA ligands for Lg were established. The association constant (K_a) measured for 7-OHPA ($(2.3\pm0.2)\times10^5$ M^{-1}) is similar to the value for the PA ($(3.8\pm0.1)\times10^5$ M^{-1}) [18]. In contrast, K_a for 3-OHPA ($(1.1\pm0.3)\times10^6$ M^{-1}) is approximately three-time larger than that of PA, while for 16-OHPA the value ($(2.3\pm0.2)\times10^4$ M^{-1}) is an order of magnitude smaller.

The results of the binding measurements indicate that the addition of an -OH group to the acyl chain of PA can influence its affinity for Lg in solution, but the effect is sensitive to the position on the chain. The slight enhancement in affinity of 3-OHPA (compared to PA) may be due to the formation of intermolecular H-bonds. However, it is not possible to draw any firm conclusions due to uncertainty in the influence of solvent reorganization on the thermodynamic parameters for the association reaction. For this reason it is also not possible to ascertain whether intermolecular H-bonds exist for the Lg complexes of 7-OHPA or 16-OHPA.

Efforts to quantify the dissociation kinetics of the (Lg + X-OHPA) complexes in solution using SPR spectroscopy were unsuccessful. The dissociation kinetics for the (Lg + 3-OHPA), (Lg + 7-OHPA) and (Lg + 16-OHPA) complexes are significantly faster

than those reported for the (Lg + PA) complex [10] and too fast to accurately measure (data not shown).

Stability of the gaseous (Lg + X-OHPA)$^{7-}$ ions

Time-resolved BIRD measurements were performed on the (Lg + X-OHPA)$^{7-}$ ions at temperatures ranging from 48 to 83°C. As illustrated in Figure 3, the loss of neutral X-OHPA was observed for all three (Lg + X-OHPA)$^{7-}$ ions (eq 1a). The loss of deprotonated X-OHPA was also observed, as a minor pathway, for the (Lg + 3-OHPA)$^{7-}$ and (Lg + 16-OHPA)$^{7-}$ ions (eq 1b).

$$(\text{Lg} + \text{X-OHPA})^{7-} \rightarrow \text{Lg}^{7-} + \text{X-OHPA} \quad (1a)$$

$$\rightarrow \text{Lg}^{6-} + \text{X-OHPA}^{-} \quad (1b)$$

The loss of deprotonated ligand from the (Lg + 3-OHPA)$^{7-}$ ions was not unexpected. The –OH group, which is in close proximity to the carboxyl group, will enhance the acidity (i.e., lower the gas-phase acidity (GA)) of the ligand (compared to PA) through an inductive effect and through the formation of an intramolecular H-bond between the –OH group and the carboxylate oxygens. The absence of the deprotonated ligand pathway for the (Lg + 7-OHPA)$^{7-}$ ions indicates that the –OH group is too remote from the carboxyl group to influence (through bond or through space) the GA of the ligand. The observation of the loss of deprotonated ligand from (Lg + 16-OHPA)$^{7-}$ is intriguing, particularly given the absence of this pathway for the (Lg + 7-OHPA)$^{7-}$ ions. The reduction in GA of 16-OHPA must involve the formation of an intramolecular H-bond. However, if the acyl chain is initially buried in the cavity, as is believed to be the case for both the *fast* and the *slow* components, such an interaction in the dissociative *TS* seems unlikely. Instead, and

as supported by the kinetic data, *vide infra*, this pathway likely originates from a third structure, possibly one in which the acyl chain is located outside of the cavity.

Shown in Figure 4 are plots of the natural log of the normalized abundance (Ab/Ab_{total}) of the (Lg + X-OHPA)$^{7-}$ ions versus reaction time (t) measured for each ligand at the temperatures indicated. All of the kinetic plots exhibit non-linear behaviour, consistent with the presence of multiple, kinetically distinct structures. The kinetic data measured for the dissociation of the (Lg + 7-OHPA)$^{7-}$ ion, which proceeds exclusively by the loss of neutral ligand, are well described by a double exponential function (eq 2):

$$Ab/Ab_{total} = X_{f,0}\mathrm{e}^{-k_f t} + X_{s,0}\mathrm{e}^{-k_s t} \quad (2)$$

where $X_{f,0}$ and $X_{s,0}$ correspond to the initial fractions of the two components (i.e., the *fast* and *slow* components, respectively) and k_f and k_s are the dissociation rate constants, respectively. These results indicate the presence of two dominant, non-interconverting structures [10]. BIRD of the (Lg + PA)$^{7-}$ ion yielded similar results [10]. Based on the results of MD simulations performed on (Lg + PA)$^{7-}$, it was suggested that the main structural difference between the *fast* and *slow* structures is the position of the flexible EF loop of Lg [10]. In the *fast* structures, the loop is in an "open" position, such that the PA is stabilized mainly by protein-lipid interactions, while in the *slow* structures the loop is in a "closed" position and H-bonds between the ligand carboxyl group and Lg also contribute to the stability of the complex.

The kinetic data measured for the (Lg + 3-OHPA)$^{7-}$ and (Lg + 16-OHPA)$^{7-}$ ions can also be described reasonably well by a double exponential function. In the case of (Lg + 3-OHPA)$^{7-}$, it was found that both the *fast* and *slow* components dissociate via parallel pathways leading to the loss of neutral or deprotonated ligand (eqs 3a-d):

$k_{f,N}$

$$(\text{Lg} + \text{3-OHPA})_f^{7-} \rightarrow \text{Lg}^{7-} + \text{3-OHPA} \quad (3a)$$

$$\xrightarrow{k_{f,C}} \text{Lg}^{6-} + \text{3-OHPA}^{-} \quad (3b)$$

$$(\text{Lg} + \text{3-OHPA})_s^{7-} \xrightarrow{k_{s,N}} \text{Lg}^{7-} + \text{3-OHPA} \quad (3c)$$

$$\xrightarrow{k_{s,C}} \text{Lg}^{6-} + \text{3-OHPA}^{-} \quad (3d)$$

Show in Figure S1 are plots of the fractional abundance of the Lg^{6-} product ion (i.e., $Ab_{(Lg6-)}/Ab_{total}$) and the product ion abundance ratio ($Ab_{(Lg6-)}/Ab_{(Lg7-)}$) versus *t* measured at 57, 65, and 81 °C. It can be seen that while $Ab_{(Lg6-)}/Ab_{total}$ increases with *t*, the $Ab_{(Lg6-)}/Ab_{(Lg7-)}$ ratio is essentially constant. These results confirm the operation of parallel dissociation pathways for both the *fast* and the *slow* components with similar or identical branching ratios (i.e., ratio of the dissociation rate constants), eq 4:

$$k_{f,C}/k_{f,N} = k_{s,C}/k_{s,N} = Ab_{(Lg6-)}/Ab_{(Lg7-)} \quad (4)$$

where $k_{f,C}$ and $k_{f,N}$ are rate constants for loss of deprotonated and neutral 3-OHPA from the *fast* component, respectively, and $k_{s,C}$ and $k_{s,N}$ are rate constants for loss of deprotonated and neutral 3-OHPA from the *slow* component, respectively. It follows that the individual reaction rate constants ($k_{f,N}$, $k_{f,C}$, $k_{s,N}$ and $k_{s,C}$) can be calculated, at each temperature, from $k_{f,app}$ and $k_{s,app}$, which represent the sum of the two pathways (eqs 5a,b) and are obtained by fitting eq 6 to the kinetic data, and the measured branching ratios.

$$k_{f,app} = k_{f,N} + k_{f,C} \quad (5a)$$

$$k_{s,app} = k_{s,N} + k_{s,C} \quad (5b)$$

$$Ab/Ab_{total} = X_{f,0}e^{-k_{f,app}t} + X_{s,0}e^{-k_{s,app}t} \quad (6)$$

Plotted in Figure S2 is the fractional abundance of the Lg^{6-} product ion (i.e., $Ab_{(Lg6-)}/Ab_{total}$) versus *t* measured for $(Lg + 16\text{-OHPA})^{7-}$ at 47, 57, 65, and 76 °C. Notably, at every temperature the fraction of the Lg^{6-} product ion is essentially constant over the course of

the reaction, with an average value of ~0.1. Based on these results it is concluded that, in addition to the *fast* and the *slow* components, the $(Lg + 16\text{-}OHPA)^{7-}$ ions exists in at least one other structure, which rapidly (compared to the pathways leading to the loss of neutral ligand) dissociates by the loss of deprotonated ligand. Because this third structure is rapidly consumed at the start of the reaction, it can be neglected in the analysis of the kinetic data and k_f and k_s determined by fitting eq 2 to the experimental data.

Arrhenius plots (Figure 5) were constructed from the dissociation rate constants ($k_{f,N}$, $k_{f,C}$, $k_{s,N}$ and $k_{s,C}$) and the corresponding Arrhenius parameters are listed in Table 1. For comparison purposes, Arrhenius plots for the dissociation of the $(Lg + PA)_f^{7-}$ and $(Lg + PA)_s^{7-}$ ions are shown in Figure 5 and the parameters are listed in Table 1 [10]. Inspection of the Arrhenius parameters reveals that hydroxylation of the acyl chain of PA results in a significant increase in E_a for neutral ligand loss, 6 to 8 kcal mol^{-1} for the *fast* component and 5 to 11 kcal mol^{-1} for the *slow* component. As discussed above and elsewhere [10-12], the gaseous $(Lg + PA)_f^{7-}$ ion is believed to be stabilized predominantly by protein-lipid interactions, similar to the structure that exists in aqueous solution. Thus, the higher E_a values for the $(Lg + X\text{-}OHPA)_f^{7-}$ ions can be explained by the formation of a strong H-bond (or possibly multiple weak H-bonds) between the -OH group and Lg. Similar arguments can explain the increase in E_a values measured for the loss of neutral ligand from the *slow* components. Interestingly, the presence of the -OH group has little or no influence on the E_a for the loss of deprotonated X-OHPA from the $(Lg + 3\text{-}OHPA)^{7-}$ ions, despite the fact that the loss of neutral and deprotonated 3-OHPA occur in parallel. This observation suggests that the increase in dissociation E_a due to the

presence of intermolecular H-bond(s) is offset by a reduction in E_a resulting from Coulombic repulsion between the charged product ions (i.e., Lg^{6-} and 3-$OHPA^-$) [9,21].

Structures of the hydrated and dehydrated (Lg + X-OHPA) complexes

MD simulations were performed on the hydrated (Lg + X-OHPA) complexes, as well as the gaseous deprotonated $(Lg + X\text{-}OHPA)^{7-}$ ions, to suggest possible H-bonds involving the –OH groups. The crystal structure of the (Lg + PA) complex (PDB ID1B0O) was used as the starting structure for the (Lg + X-OHPA) complexes and the -OH groups were manually added to the acyl chain. For the hydrated (Lg + X-OHPA) complexes, all acidic and basic residues on the surface of Lg were charged (negatively or positively, respectively), and the overall charge of the complex was -8. For the gaseous $(Lg + X\text{-}OHPA)^{7-}$ ions, a charge configuration that leads to the formation of the "open" structure, in which the carboxyl group does not participate in strong H-bonds, was used (deprotonated residues: Asp^{53}, Asp^{85}, Asp^{98}, Asp^{130}, Glu^{45}, Glu^{114}, Glu^{158}) [10].

Analysis of the trajectories obtained for the $(Lg + X\text{-}OHPA)^{7-}$ ions reveals the presence of one or two intermolecular H-bonds for each ligand. For the $(Lg + 3\text{-}OHPA)^{7-}$ ion, the ligand -OH group is found to participate in a H-bond with the amide oxygen of Pro^{38}. Based on the narrow distributions of bond lengths (r) (centered at 2.7-3.1 Å) and bond angles (θ) (centered at 120°) this appears to be a relatively stable interaction (Figure 6a). The MD simulations also predict a stable H-bond between the -OH group 16-OHPA and the amide oxygen of Asp^{11} (Figure 6c). In contrast, the results of the MD simulations performed on the $(Lg + 7\text{-}OHPA)^{7-}$ ion suggest the simultaneous formation of two H-bonds between the -OH group and the amine nitrogen group ($-NH_2$) of Asn^{88} ($-NH_2$ is hydrogen acceptor) and of Asn^{90} ($-NH_2$ is hydrogen donor). Given the broad distribution

of r (centered at ~4.0 Å) and θ (centered at ~80°) (Figure 6b), the individual interactions are expected to be relatively weak. However, together, their energetic contributions to the stability of (Lg + 7-OHPA)$^{7-}$ might be expected to be similar to that of the individual H-bonds identified for the other two ligands. Because only a single charge state configuration was considered and the inability of the MD method used to account for proton migration, the intermolecular H-bonds identified in the present work cannot be viewed as more than suggestions.

Analysis of the MD trajectories obtained for the hydrated (Lg + X-OHPA) complexes reveals that the –OH groups of 3-OHPA and 7-OHPA do not participate in any strong H-bonds with Lg, this despite the fact that the cavity size and shape is similar in both the hydrated and dehydrated complexes. In contrast, a stable H-bond involving the ligand -OH group and the amide oxygen of Pro^{79} (r centered at 2.7 Å, and θ centered at 160°) was identified for the (Lg + 16-OHPA) complex (Figure 6d). These findings are surprising given that, of the three ligands, 16-OHPA exhibits the lowest affinity for Lg in aqueous solution. The lower affinity measured for16-OHPA can be reconciled with the putative intermolecular H-bond suggested from the MD results on the basis that the energetic (Gibbs energy) penalty to desolvating the ligand –OH group, which necessarily accompanies complex formation, is greater in magnitude to that corresponding to the formation of the intermolecular H-bond. However, desolvation of the –OH group must also accompany the formation of the (Lg + 7-OHPA) and (Lg + 3-OHPA) complexes in solution. Consequently, in the absence of intermolecular H-bonds, it is difficult to rationalize the finding that the affinities of these ligands for Lg are similar (or slightly higher, in the case of 3-HOPA) to that of PA. Therefore, while the modeling results, on

their own, suggest that the strong intermolecular H-bonds present in the gaseous (Lg + 3-OHPA)$^{7-}$ and (Lg + 7-OHPA)$^{7-}$ ions are absent in solution, it is seems more likely that the computational method failed to identify H-bonds that exist in the hydrated complexes.

Conclusions

The present work represents the first quantitative investigation of the energetics of intermolecular H-bonds inside a hydrophobic protein cavity. The kinetic measurements performed on the gaseous (Lg + X-OHPA)$^{7-}$ ions provide clear evidence that Lg has the capacity to form strong (5 – 11 kcal mol^{-1}) intermolecular H-bonds with the three monohydroxylated FAs. The results of MD simulations suggest that the –OH groups of 3-OHPA and 16-OHPA form a single H-bond with a backbone carbonyl oxygen, while the –OH group of 7-OHPA acts as both acceptor and donor in two H-bonds with the side chains of nearby residues. Notably, the capacity for intermolecular H-bonds within the Lg cavity, as suggested by the gas-phase measurements, does not necessarily lead to enhanced binding in aqueous solution. The affinities measured for 3-OHPA and 7-OHPA are similar to that of PA, while for 16-OHPA the affinity is an order of magnitude smaller. Taken together, the results of this study highlight the complex role of intermolecular H-bonds within hydrophobic protein cavities in the thermodynamics of protein-ligand interactions.

References

1. Pace, C.N., Shirley, B.A., McNutt, M., Gajiwala, K.: Forces contributing to the conformational stability of proteins. *FASEB J*. **10**, 75-83 (1996).
2. Efremov, R.G., Chugunov, A.O., Pyrkov, T.V., Priestle, J.P., Arseniev, A.S., Jacoby, E.: Molecular lipophilicity in protein modeling and drug design. *Curr. Med. Chem*. **14**, 393-415(2007).
3. Meyer, E.E., Rosenberg, K.J., Israelachvili, J.: Recent progress in understanding hydrophobic interactions. *Proc. Natl. Acad. Sci. USA*, **103**, 15739-15746 (2006).
4. Wang, R., Lu, Y., Fang, X., Wang, S.: An extensive test of 14 scoring functions using the PDB bind refined set of 800 protein-ligand complexes. *J. Chem. Inf. Comp. Sci*. **44**, 2114-2125 (2004).
5. Patil, R., Das, S., Stanley, A., Yadav, L., Sudhakar, A., Varma, A.K.: Optimized hydrophobic interactions and hydrogen bonding at the target-ligand interface leads the pathways of drug-designing. *PLoS One* **45**, e12029 (2010).
6. Friesner, R.A., Murphy, R.B., Repasky, M.P., Frye, L.L., Greenwood, J.R., Halgren, T.A., Sanschagrin, P.C., Mainz, D.T.: Extra precision glide: docking and scoring incorporating a model of hydrophobic enclosure for protein-ligand complexes. *J. Med. Chem*. **49**, 6177-6196 (**2006**).
7. Young, T., Abel, R., Kim, B., Berne, B., Friesner, R.A.: Motifs for molecular recognition exploiting hydrophobic enclosure in protein-ligand binding. *Proc. Natl. Acad. Sci. USA*, **104**, 808-813 (2007).

8. Kitova, E.N., Bundle, D.R., Klassen, J.S.: Partitioning of solvent effects and intrinsic interactions in biological recognition. *Angew. Chem. Int. Ed.* **43**, 4183-4186 (2004).

9. Kitova, E.N., Seo, M., Roy, P.-N., Klassen, J.S.: Elucidating the intermolecular interactions within a desolvated protein-ligand complex. An experimental and computational study. *J. Am. Chem. Soc.* **130**, 1214-1226 (2008).

10. Liu, L., Bagal, D., Kitova, E.N., Schnier, P.D., Klassen, J.S.: Hydrophobic protein-ligand interactions preserved in the gas phase. *J. Am. Chem. Soc.* **131**, 15980-15981 (2009).

11. Liu, L., Michelsen, K., Kitova, E.N., Schnier, P.D., Klassen, J.S.: Evidence that water can reduce the kinetic stability of protein-hydrophobic ligand interaction. *J. Am. Chem. Soc.* **132**, 17658-17660 (2010).

12. Liu, L., Michelsen, K., Kitova, E.N., Schnier, P.D., Klassen, J.S.: Energetics of lipid binding in a hydrophobic protein cavity. *J. Am. Chem. Soc.* **134**, 3054-3060 (2012).

13. Deng, L., Broom, A., Kitova, E.N., Richards, M.R., Zheng, R.B., Shoemaker, G.K., Meiering, E.M., Klassen, J.S.: Kinetic stability of the streptavidin-biotin interaction enhanced in the gas phase. *J. Am. Chem. Soc.* **134**, 16586-16596 (2012).

14. Deng, L., Kitova, E.N., Klassen, J.S.: Dissociation kinetics of the streptavidin-biotin interaction measured using direct electrospray ionization mass spectrometry analysis. *J. Am. Soc. Mass. Spectrom*. **24**, 49-56 (2013).

15. Kontopidis, G.; Holt, C.; Sawyer, L: Invited Review: β-lactoglobulin: binding properties, structure, and function. *J. Dairy Sci*. **87**, 785-796 (2004).

16. Qin, B.Y.; Bewley, M.C.; Creamer, L.K.; Baker, H.M.; Baker, E.N.; Jameson, G.B.: Structure basis of the Tanford transition of bovine β-lactoglobulin. *Biochemistry* **37**, 14014-14023 (1998).

17. Qvist, J.; Davidovic, M.; Hamelberg, D.; Halle, B.: A dry ligand-binding cavity in a solvated protein. *Proc. Natl. Acad. Sci. USA*, **105**, 6296-6301 (2008).

18. Liu, L., Kitova, E.N., Klassen, J.S.: Quantifying protein-fatty acid interactions using electrospray ionization mass spectrometry. *J. Am. Soc. Mass. Spectrom*. **22**, 310-318 (2011).

19. Dunbar, R.C., McMahon, T.B.: Activation of unimolecular reactions by ambient blackbody radiation. *Science*, **279**, 194-197 (1998).

20. Price, W.D., Schnier, P.D., Jockusch, R.A., Strittmatter, E.R., Williams, E.R.: Unimulecular reaction kinetics in the high-pressure limit without collisoins. *J. Am. Chem. Soc*. **118**, 10640-10644 (1996).

21. Sun, J., Kitova, E.N., Klassen, J.S.: Method for stabilizing protein-ligand complexes in nanoelectrospray ionization mass spectrometry. *Anal. Chem*. **79**, 416-425 (2007).

22. Bagal, D., Kitova, E.N., Liu, L., El-Haweit, A., Schnier, P.D., Klassen, J.S.: Gas phase stabilization of noncovalent protein complexes formed by electrospray ionization. *Anal. Chem*. **81**, 7801-7806 (2009).

Table 1. Arrhenius parameters (E_a, A) determined for the loss of neutral and deprotonated ligand (X-OHPA) from the gaseous $(Lg + X\text{-}OHPA)_f^{7-}$ and $(Lg + X\text{-}OHPA)_s^{7-}$ ions.[a]

Ligand	E_a (kcal mol^{-1})	A (s^{-1})
Fast		
PA	16.2 ± 0.3 [b]	$10^{10.2\pm0.2}$ [b]
3-OHPA (neutral)	22.3 ± 0.4	$10^{13.6\pm0.3}$
3-OHPA (deprotonated)	16.7 ± 0.5	$10^{9.4\pm0.4}$
7-OHPA	22.2 ± 0.5	$10^{13.5\pm0.2}$
16-OHPA	23.9 ± 0.2	$10^{14.6\pm0.1}$
Slow		
PA	23.8 ± 0.9 [b]	$10^{14.2\pm0.6}$ [b]
3-OHPA (neutral)	28.3 ± 1.7	$10^{16.0\pm 1.1}$
3-OHPA (deprotonated)	21.8 ± 1.3	$10^{11.4\pm0.9}$
7-OHPA	35.1 ± 0.6	$10^{20.8\pm0.4}$
16-OHPA	33.3 ± 1.2	$10^{19.6\pm 0.7}$

a. The reported errors are one standard deviation. b. Values taken from reference [10].

Figure captions

Figure 1. (a) Crystal structure of Lg complex with palmitic acid (PDB 1B0O). Amino acid residues that line the hydrophobic cavity are indicated. Structures of (b) PA, (c) 3-OHPA, (d) 7-OHPA, and (e) 16-OHPA.

Figure 2. ESI mass spectra acquired for aqueous solutions (pH 8.5, 25 °C) of (a) Lg (15 μM), 3-OHPA (9 μM), (b) Lg (12 μM), 7-OHPA (9 μM), and (c) Lg (15 μM), 16-OHPA (24 μM).Each solution contained 10 mM ammonium acetate and 10 mM imidazole.

Figure 3. Illustrative BIRD mass spectra measured for $(Lg + 3\text{-}OHPA)^{7-}$ at a reaction temperature of 76 °C and a reaction time of (a) 2 s and (b) 20 s; for $(Lg + 7\text{-}OHPA)^{7-}$ at 58 °C and (c) 10 s, and (d) 160 s; for $(Lg + 16\text{-}OHPA)^{7-}$ at 66 °C and (e) 20 s, and (f) 50 s.

Figure 4. Plots of the natural logarithm of the normalized abundance (Ab/Ab_{total}) of (a) $(Lg + 3\text{-}OHPA)^{7-}$, (b) $(Lg + 7\text{-}OHPA)^{7-}$ and (c) $(Lg + 16\text{-}OHPA)^{7-}$ versus reaction time at the temperatures indicated.

Figure 5. Arrhenius plots for the loss of neutral ligand from the $(Lg + X\text{-}OHPA)_f^{7-}$ (solid circle) and $(Lg + X\text{-}OHPA)_s^{7-}$ ions (open circle) for X-OHPA = 3-OHPA (●), 7-OHPA (●), 16-OHPA (●), PA (●); and Arrhenius plots for the loss of charged ligand from $(Lg + 3\text{-}OHPA)_f^{7-}$ (●) and $(Lg + 3\text{-}OHPA)_s^{7-}$ (o).

Figure 6. Representative structures obtained from MD simulations for gaseous (a) $(Lg + 3\text{-}OHPA)^{7-}$, (b) $(Lg + 7\text{-}OHPA)^{7-}$, (c) $(Lg + 16\text{-}OHPA)^{7-}$ ions, and (d) hydrated (Lg+16-OHPA) complex. Number of occurrences (*N*) of H-bond distances and angles (inset), obtained by MD simulations for the (a) 3-OHPA

C3 OH/Pro^{38} O (amide oxygen) interaction in the (Lg + 3-OHPA)$^{7-}$ ion; (b) 7-OHPA C7 OH/Asn^{88} NH_2 (hydrogen acceptor) and 7-OHPA C7 OH/Asn^{90} H_2N (hydrogen donor) interactions in the (Lg + 7-OHPA)$^{7-}$ ion; (c) 16-OHPA C16 OH/Asp^{11} O (amide oxygen) interaction in the (Lg + 16-OHPA)$^{7-}$ ion, and (d) 16-OHPA C16 OH/Pro^{79} O (amide oxygen) interaction in the hydrated (Lg + 16-OHPA) complex.

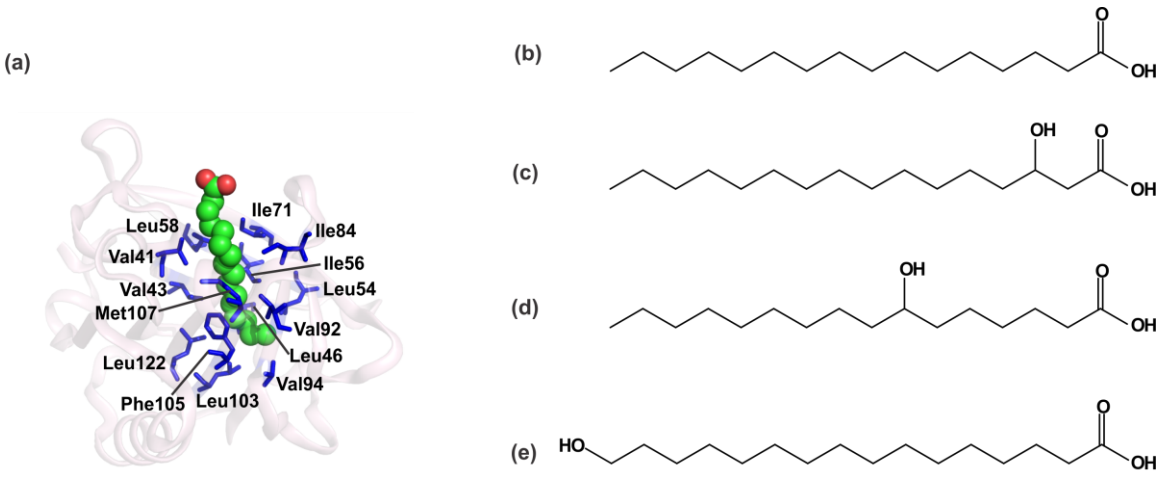
(a)
Ile71
Leu58
Ile84
Val41
Ile56
Val43
Leu54
Met107
Val92
Leu46
Leu122
Val94
Phe105
Leu103
(b)
O
OH
(c)
OH
O
OH
(d)
OH
O
OH
(e)
HO
O
OH

Figure 1

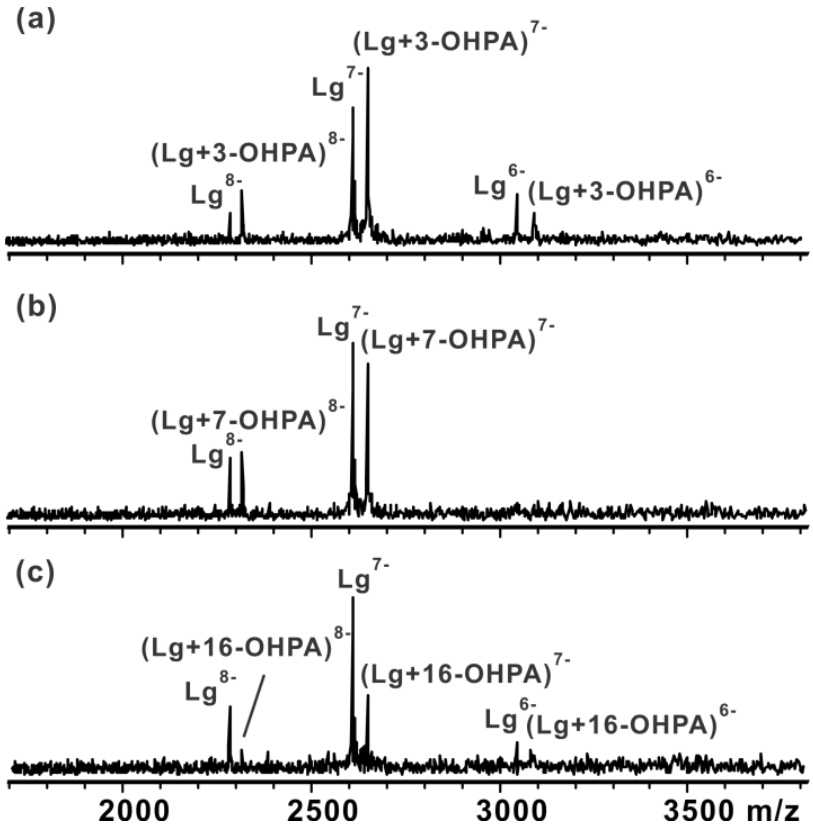
(a)
(Lg+3-OHPA)7-
Lg7-
(Lg+3-OHPA)8-
Lg8-
Lg6-
(Lg+3-OHPA)6-
(b)
Lg7-
(Lg+7-OHPA)7-
(Lg+7-OHPA)8-
Lg8-
(c)
Lg7-
(Lg+16-OHPA)8-
Lg8-
(Lg+16-OHPA)7-
Lg6-
(Lg+16-OHPA)6-
2000
2500
3000
3500 m/z

Figure 2

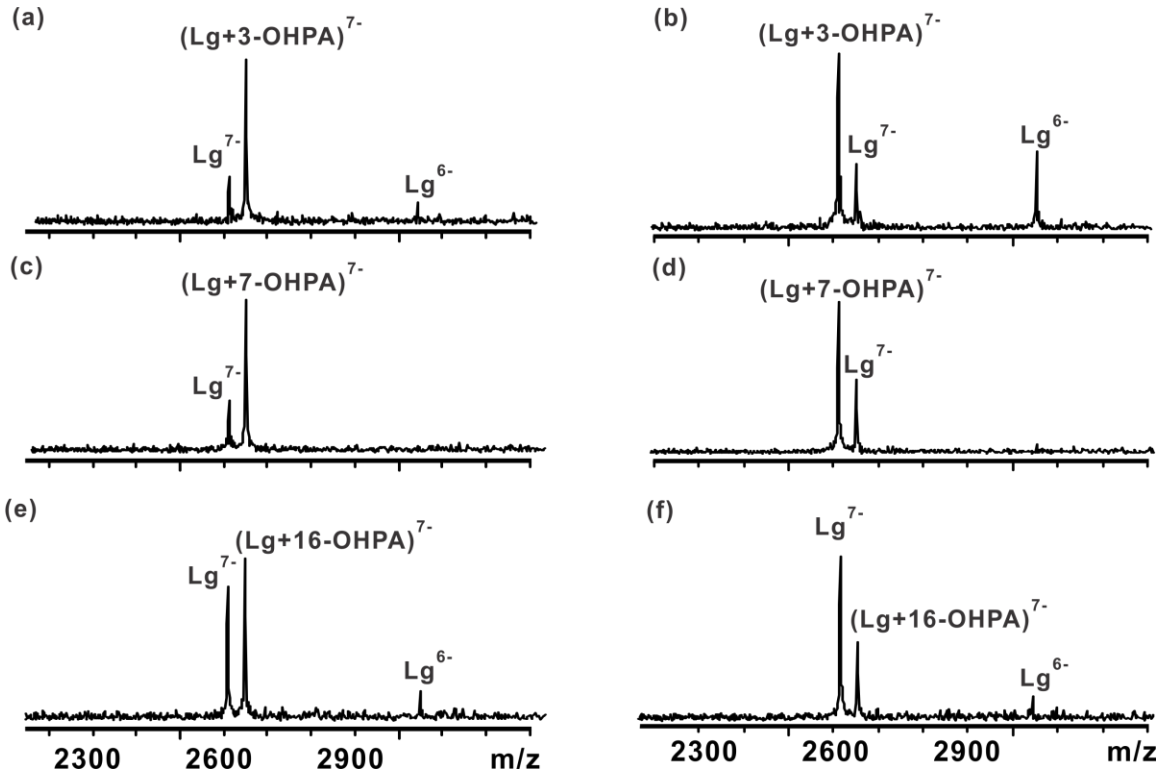
(a)
(Lg+3-OHPA)7-
Lg7-
Lg6-
(b)
(Lg+3-OHPA)7-
Lg7-
Lg6-
(c)
(Lg+7-OHPA)7-
Lg7-
(d)
(Lg+7-OHPA)7-
Lg7-
(e)
(Lg+16-OHPA)7-
Lg7-
Lg6-
(f)
Lg7-
(Lg+16-OHPA)7-
Lg6-
2300
2600
2900
m/z
2300
2600
2900
m/z

Figure 3

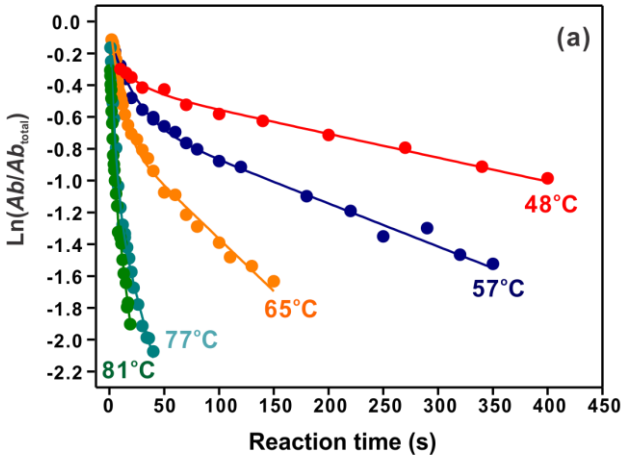
(a)
Ln(Ab/Ab_total)
Reaction time (s)
48°C
57°C
65°C
77°C
81°C

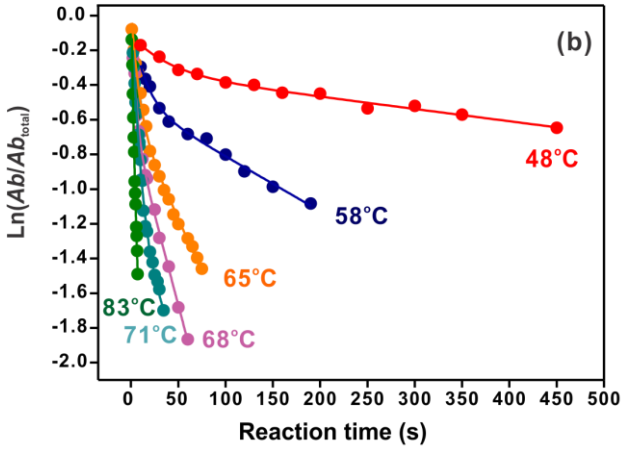
(b)
Ln(Ab/Ab_total)
Reaction time (s)
48°C
58°C
65°C
83°C
71°C
68°C

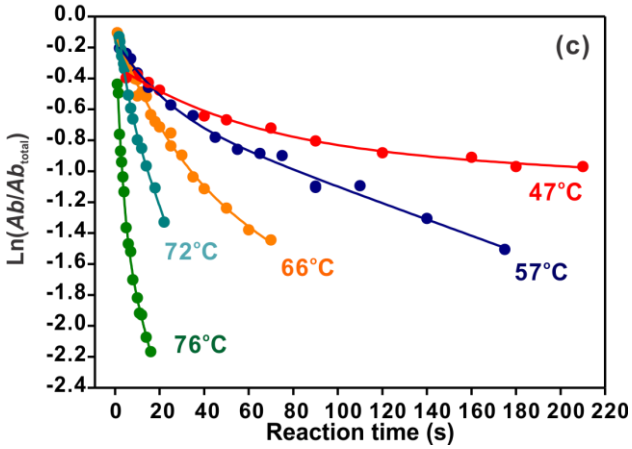
(c)
Ln(Ab/Ab_total)
Reaction time (s)
47°C
57°C
66°C
72°C
76°C

Figure 4

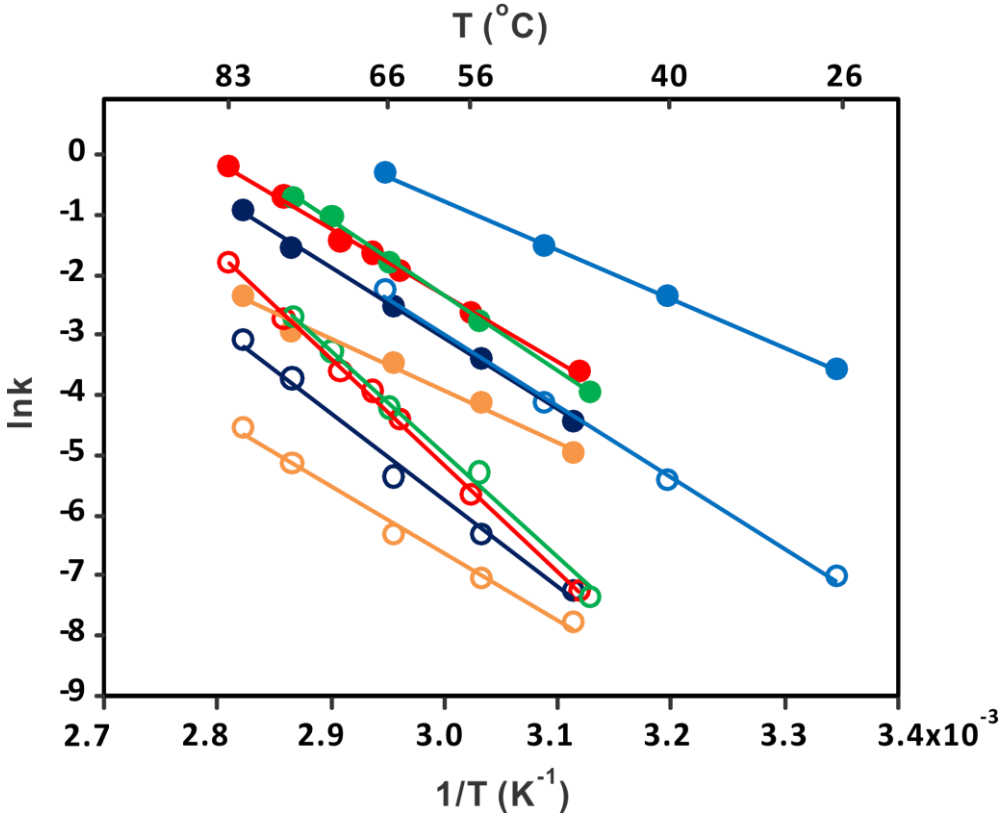

Figure 5

(a)

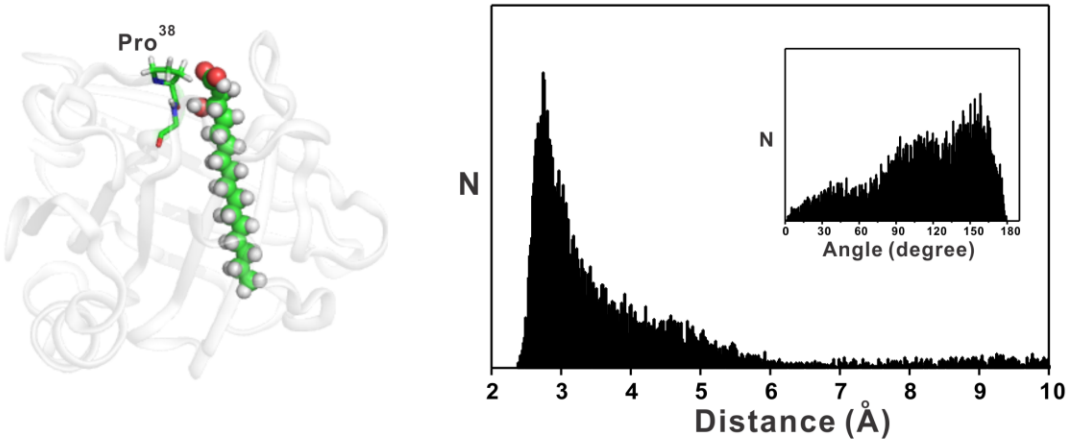
Pro38
N
2 3 4 5 6 7 8 9 10
Distance (Å)
N
0 30 60 90 120 150 180
Angle (degree)

(b)

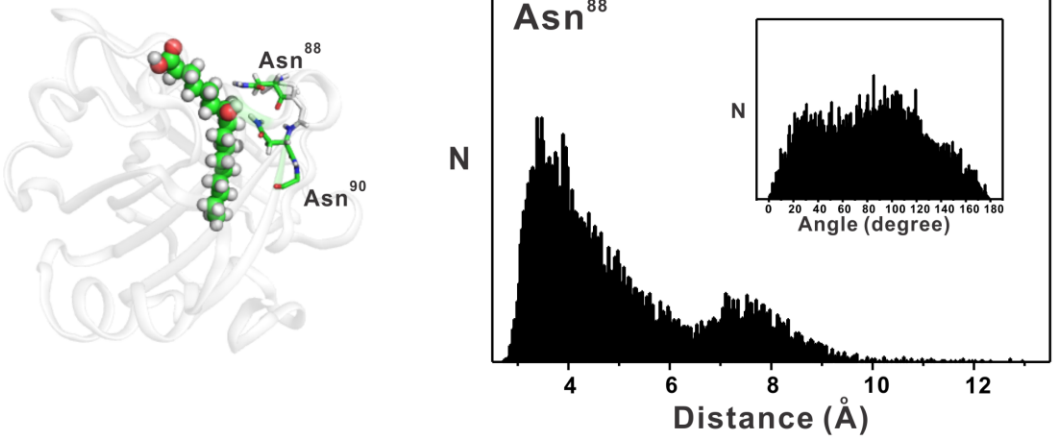
Asn88
Asn90
Asn88
N
4 6 8 10 12
Distance (Å)
N
0 20 40 60 80 100 120 140 160 180
Angle (degree)

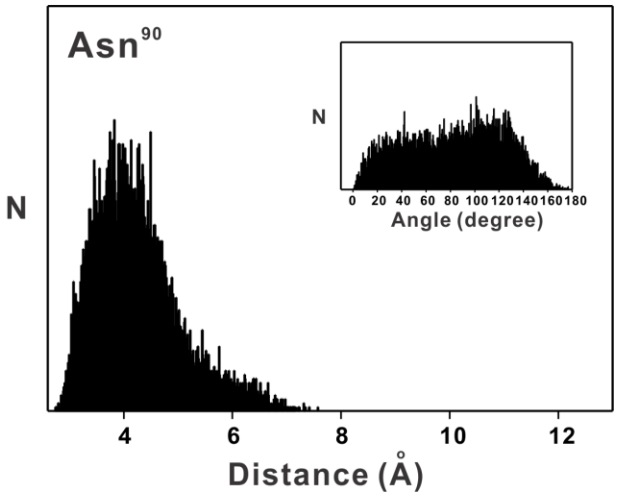
Asn90
N
4 6 8 10 12
Distance (Å)
N
0 20 40 60 80 100 120 140 160 180
Angle (degree)

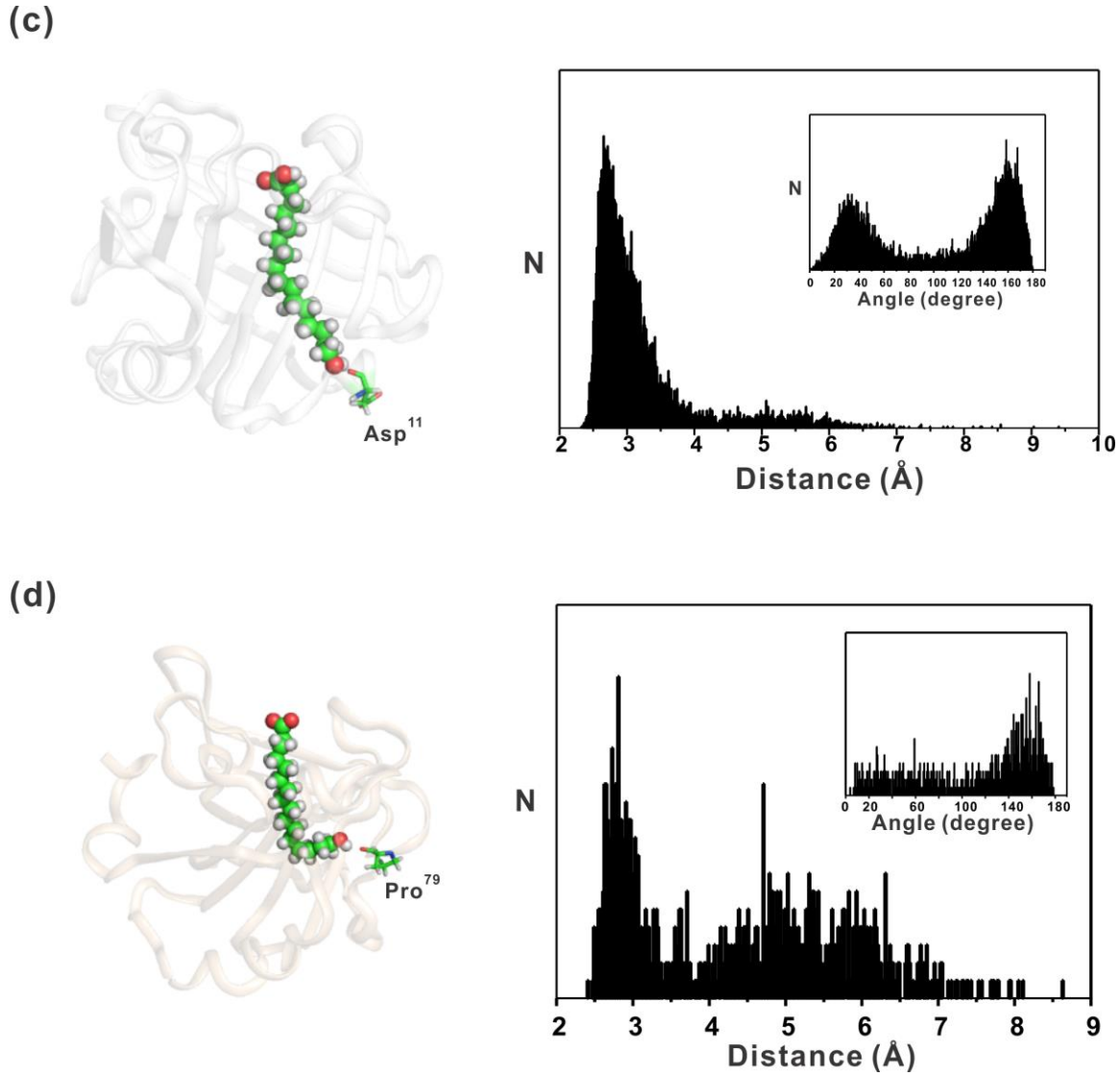
(c)
Asp11
N
Distance (Å)
Angle (degree)
(d)
Pro79
N
Distance (Å)
Angle (degree)

Figure 6

Supplementary Information for:

Energetics of Intermolecular Hydrogen Bonds in a Hydrophobic Protein Cavity

Lan Liu, Alyson Baergen, Klaus Michelsen, Elena N. Kitova, Paul D. Schnier and John S. Klassen

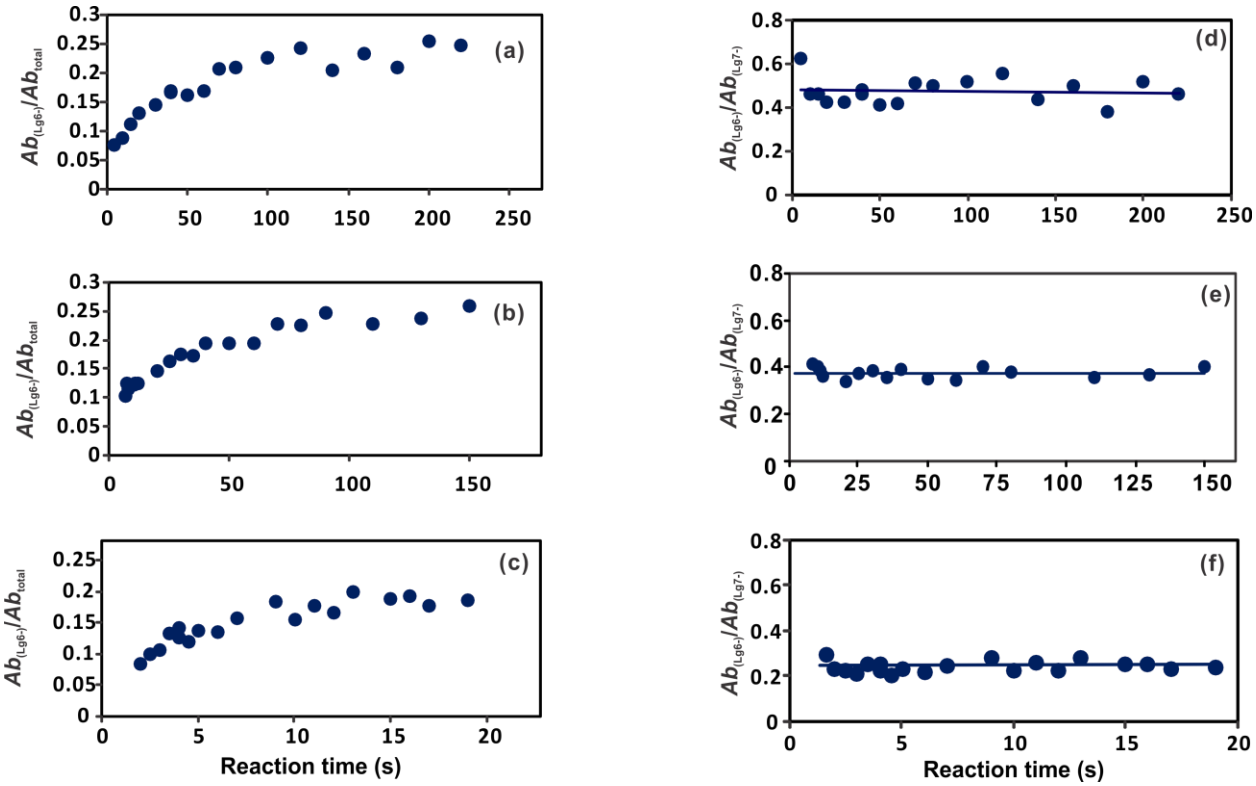

Figure S1. Plots of the fractional abundance of Lg^{6-} ($Ab_{(Lg6-)}/Ab_{total}$) versus reaction time measured for the dissociation of $(Lg + 3\text{-}OHPA)^{7-}$ ions at (a) 57 °C, (b) 65 °C and (c) 81 °C. Plots of the abundance ratio of Lg^{6-} and Lg^{7-} ($Ab_{(Lg6-)}/Ab_{(Lg7-)}$) versus reaction time measured for the dissociation of $(Lg + 3\text{-}OHPA)^{7-}$ ions at (d) 57 °C, (e) 65 °C and (f) 81 °C.

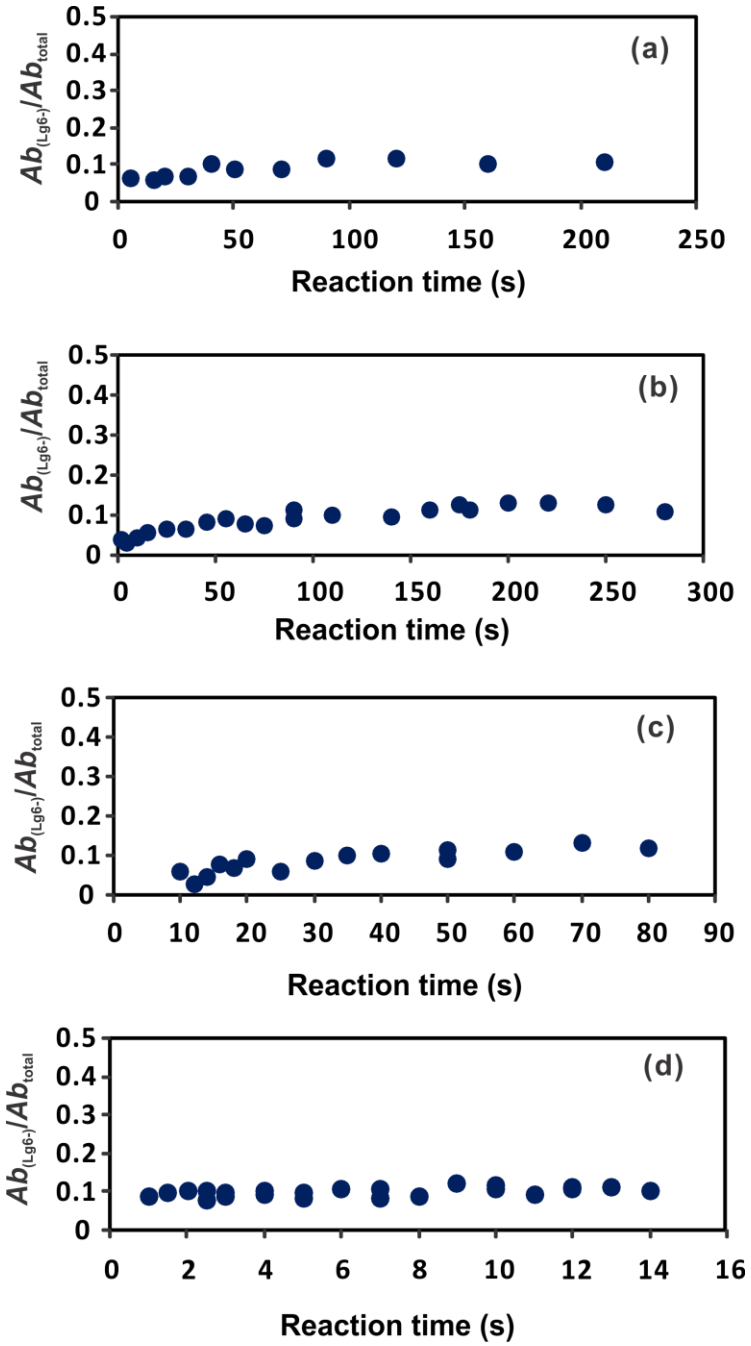

Figure S2. Plots of the fractional abundance of Lg^{6-} ($Ab_{(Lg6-)}/Ab_{total}$) versus reaction time measured for the dissociation of $(Lg + 16\text{-}OHPA)^{7-}$ ions at (a) 47 °C, (b) 57 °C, (c) 65 °C and (d) 76 °C.